



## Valorization of fruit wastes (pistachio shells) as adsorbent for the removal of Zn from aqueous solutions under adverse acidic conditions

C.A. Aggelopoulos<sup>a,\*</sup>, E. Moschopoulou<sup>a</sup>, P.G. Klepetsanis<sup>a,b</sup>, C.D. Tsakiroglou<sup>a,\*</sup>

<sup>a</sup>Foundation for Research and Technology Hellas-Institute of Chemical Engineering Sciences (FORTH/ICE-HT), 26504 Patras, Greece, Tel. +302610965205; Fax: +302610965223; emails: caggelop@iceht.forth.gr (C.A. Aggelopoulos), ctsakir@iceht.forth.gr (C.D. Tsakiroglou), elenmosch@yahoo.gr (E. Moschopoulou)

<sup>b</sup>University of Patras, Department of Pharmacy, 26504 Patras, Greece, email: klepe@upatras.gr

Received 24 November 2016; Accepted 20 March 2017

### ABSTRACT

Low-cost adsorbents (LCAs) were prepared from pistachio shells after minor treatment over the temperature range 300°C–500°C, under nitrogen, carbon dioxide, and air atmosphere. The LCAs were evaluated with respect to their capacity to remove zinc (Zn) from aqueous solutions under adverse acidic conditions (pH < 4), where the dissolution of oxides/hydroxides is favored and low sorption capacity of the raw material is expected. Potential changes of the sorption capacity were interpreted in terms of: (i) the surface functional groups identified with attenuated total reflection Fourier transform infrared spectra; (ii) the pore space morphology quantified by N<sub>2</sub> sorption data, Hg intrusion porosimetry, and scanning electron microscopy images; (iii) the phase crystallinity analyzed with X-ray diffraction; and (iv) the thermal stability recorded with thermogravimetric analysis. For all aqueous solutions, including those having the highest initial Zn concentration (100 mg/L), the maximum Zn removal efficiency was observed for the air-activated adsorbents at 500°C and 400°C. In contrast, for the N<sub>2</sub>- and CO<sub>2</sub>-activated adsorbents, the Zn removal efficiency was comparable with that of the raw pistachio shells. For air-activated adsorbents, the Zn removal efficiency was enhanced with the activation temperature and holding time increasing, while no effect of the heating rate on adsorbent sorption capacity was evident. The characteristics of the investigated adsorbents were found fully compatible with the observed Zn sorption capacity and potential sorption mechanisms. Specifically, the enhancement of the sorption capacity of air-treated adsorbents might be due to: (i) the higher pore surface area and volume associated with physical sorption; (ii) the presence of mineral phases (calcite) triggering the metal precipitation; and (iii) the presence of oxygen-rich functional groups associated with complexation and/or electrostatic attraction. The equilibrium sorption data sets of raw pistachio shells were fitted satisfactorily to both Langmuir and Freundlich isotherms, whereas the corresponding data sets of air-activated adsorbents were better fitted to Langmuir isotherm.

**Keywords:** Zinc; Adsorption; Heavy metals; Biomass; Pyrolysis; Activation

### 1. Introduction

Among the various methods that are available for wastewater treatment (e.g., coagulation, foam flotation, filtration, aerobic and anaerobic treatment, advanced oxidation processes, adsorption, microbial reduction,

activated sludge), adsorption stands out because of its convenience, ease of operation, and simplicity of design [1,2].

One of the most efficient adsorbents used for water pollution control is the activated carbon (AC), which is usually prepared from carbonaceous materials (e.g., coal, lignite, wood, etc.) through physical or chemical activation [3–5]. AC has been found to be a versatile adsorbent, which can remove diverse types of pollutants such as metal ions, anions, dyes, phenols, pharmaceuticals, pesticides, humic substances,

\* Corresponding author.

chlorinated hydrocarbons, and many other chemicals and organisms [6–8]. In spite of its abundant uses, its applications are sometimes restricted due to its high cost and regeneration problems. In this context, researchers are looking for low-cost alternative adsorbents, where cost factors play a major role [9]. Low-cost adsorbents (LCAs) can be prepared from a wide variety of raw materials, which are abundant and cheap, have high organic (carbon) content, and are capable of being activated easily [10]. The preparation of LCAs from agro-industrial wastes has several advantages, mainly of economic and environmental nature. A wide variety of raw materials such as residual stalks, straw, leaves, roots, rice husk, potatoes, orange seeds, nut or seed shells, waste wood, and animal husbandry waste have been used as low-cost alternative adsorbents [11–17]. These materials have been used either in their natural form or after some physical or chemical modification (e.g., slow pyrolysis).

During the last few years, pistachio shells (PI) have been used after either physical activation in the temperature range 600°C–1,200°C or chemical activation [18–23]. However, only in a few studies the potential to use PI as raw material for the production of LCAs after a minor treatment (e.g., pyrolysis in the temperature range 300–600°C) is emphasized [24–26]. For instance, Turan and Mesci [24] studied the removal of zinc (Zn) from water by using PI in their natural form and found the values of adsorbent dosage, pH, and contact time that maximize the Zn removal efficiency. In addition, Komnitsas et al. [25] investigated the removal of Pb and Cu from water by using the biochar produced from PI after slow pyrolysis under N<sub>2</sub> atmosphere, in the temperature range 250°C–650°C, and found that the temperature of pyrolysis affects positively the Pb and Cu sorption capacity of biochar. Nevertheless, limited attention has been paid on the preparation and use of LCA under adverse conditions of mild activation (low energy consumption) of raw material and low pH (<4) [24].

The goal of the present study is to investigate the feasibility of using PI, either in their natural state or after some minor treatment, for the removal of Zn<sup>2+</sup> from acidic water. PI were physically activated in the temperature range 300°C–500°C under inert (N<sub>2</sub>) and oxidizing (air, CO<sub>2</sub>) atmospheres. Raw material and produced adsorbents were characterized by a variety of techniques such as: N<sub>2</sub> adsorption, Hg porosimetry, attenuated total reflection Fourier transform infrared (ATR-FTIR) spectroscopy, scanning electron microscopy (SEM), X-ray diffraction (XRD), and thermogravimetric analysis/derivative thermogravimetric (TGA/DTG). Equilibrium Zn<sup>2+</sup> adsorption experiments were conducted for various initial Zn<sup>2+</sup> concentrations (5–100 mg/L) by adjusting the initial pH value equal to 3.7. The effects of the gas type, activation temperature, heating rate (HR), holding time (HT), and initial Zn<sup>2+</sup> concentration on the metal removal efficiency were examined.

## 2. Materials and methods

### 2.1. Materials

Pistachio-nut shells originating from Aegina Island (Greece) were used as raw materials. The pistachio is one of the favorite tree nuts worldwide produced in orchards of *Pistacia vera* L., and it is widely cultivated in the Middle East, Mediterranean countries, and United States [27]. The

shells were washed with warm, distilled water to remove salt, dried in an oven (Binder) at 110°C for 24 h to remove the moisture, crushed with a planetary ball mill (Retsch S1), and then sieved on a mechanical shaker (Fritsch) to a size range 1–2 mm. Zn(NO<sub>3</sub>)<sub>2</sub>·4H<sub>2</sub>O was purchased from Merck (Darmstadt, Germany) and used without further purification.

### 2.2. Physical activation process

Physical activation of the raw shells was done by heating them over the temperature range 300°C–500°C, under inert (nitrogen) or oxidizing (carbon dioxide, air) atmospheres, respectively. The physical activation with nitrogen and carbon dioxide were carried out in a vertical quartz reactor, which was placed in an electrical furnace. During the process, about 1.5 g of raw material was used to prepare the adsorbents. The gas (i.e., nitrogen or carbon dioxide) was injected continuously through the reactor at a flow rate of 80 cm<sup>3</sup>/min. The furnace temperature was increased at a rate of 5°C/min or 10°C/min, from room temperature to 300°C, 400°C, and 500°C and held at this temperature for 30 or 60 min. The physical activation with air was carried out in a laboratory furnace (KEL) at temperatures varying between 300°C and 500°C, using porcelain capsules. The HR was set at 5°C/min or 10°C/min, and the HT of the feedstock at each temperature (i.e., 300°C, 400°C, and 500°C) was 30 or 60 min. The produced adsorbents were then removed from the furnace, cooled, weighted, and stored in airtight plastic containers. The yield of adsorbent production was based on the initial and final mass of materials and calculated by the relationship:

$$\text{Yield}(\%) = \frac{\text{Weight of produced adsorbent}}{\text{Weight of pistachio shell}} \times 100 \quad (1)$$

### 2.3. Characterization of adsorbent

The structural, physical, and chemical properties of both the raw material and produced adsorbents were determined by several characterization techniques such as N<sub>2</sub> adsorption, mercury intrusion porosimetry (MIP), SEM, XRD, TGA/DTG, and ATR-FTIR spectroscopy. The specific surface area of the samples was measured with a N<sub>2</sub> adsorption analyzer (Micromeritics Gemini) by using the Brunauer–Emmett–Teller (BET) method. The mercury intrusion/curves of adsorbents were measured with a PoreMaster 60 (Quantachrome Ltd., USA) porosimeter. The morphology of the adsorbents was characterized by field-emission SEM (FE-SEM; Zeiss SUPRA 35VP-FEG) operating at 5 keV. The crystallinity of materials was identified by XRD in a Bruker D8 advanced instrument operating with Ni-filtered Cu Ka1 radiation ( $\lambda = 0.154059$  nm). The thermogravimetric measurements (TGA/DTG) were carried out in a TA Instruments Q50 thermogravimetric analyzer equipped with a quartz reactor, over the temperature range 25°C–700°C, under air/argon atmosphere, at a flow rate of 40 mL/min and HR of 5°C/min. ATR-FTIR spectra were obtained at a spectral resolution of 4 cm<sup>-1</sup> and wave numbers 400–4,000 cm<sup>-1</sup> by using a Nicolet 850FT-IR spectrometer. ATR-FTIR is a non-destructive method, and solid or liquid samples can be analyzed without the necessity of any pretreatment.

#### 2.4. Equilibrium adsorption experiments

Aqueous solutions were prepared at various Zn concentrations (5, 10, 20, 40, 80, and 100 mg/L) by dissolving  $\text{Zn}(\text{NO}_3)_2 \cdot 4\text{H}_2\text{O}$  in distilled water. The initial pH of solutions was adjusted to acidic conditions (i.e., pH = 3.7) by adding  $\text{H}_2\text{SO}_4$  solution of concentration  $5.0 \times 10^{-5}$  M. Equilibrium sorption experiments were carried out by placing 0.1 g of dry adsorbent with 10 mL of Zn solution in tightly sealed glass bottles and shaking them on an overhead shaker at a speed of 12 rpm, and room temperature for 48 h. After that, liquid samples were collected from the bottles, filtered through 0.45  $\mu\text{m}$  Whatman filters, and the Zn concentration was measured by atomic absorption spectroscopy (Perkin Elmer Analyst 300). The Zn removal efficiency, RE(%), was defined by the following equation:

$$\text{RE}(\%) = \left[ \frac{C_0 - C_f}{C_0} \right] \times 100 \quad (2)$$

where  $C_0$  and  $C_f$  are the initial (before adsorption) and final (after adsorption)  $\text{Zn}^{2+}$  concentration in aqueous solution, respectively. All equilibrium experiments were carried out in duplicate, and the  $\text{Zn}^{2+}$  concentration of each sample was regarded equal to the mean value of the two measurements. Furthermore, the measured concentration of Zn in blank tests (without adsorbent) remained identical after 48 h, indicating that no metal precipitation took place.

### 3. Results and discussion

#### 3.1. $\text{N}_2$ adsorption and Hg porosimetry measurements

The physical properties of raw PI and adsorbents produced after their treatment with various gases (i.e.,  $\text{N}_2$ ,  $\text{CO}_2$ , air) at three temperatures (i.e., 300°C, 400°C, 500°C) are summarized in Table 1. In general, the adsorbents produced from air-heated PI revealed higher surface area compared with that of adsorbents produced from  $\text{N}_2$ - and  $\text{CO}_2$ -heated PI at 400°C. Furthermore, the specific surface area of all adsorbents has the tendency to increase with the temperature increasing from 300°C to 500°C. This increase becomes more evident in the case of air-activated adsorbents (Table 1). The pore diameter distributions of raw and air-treated materials, in the pore size range  $0.004 \mu\text{m} < D < 10 \mu\text{m}$  (Fig. 1(b)), were determined with differentiation and normalization of the cumulative mercury intrusion curves (Fig. 1(a)), measured with the Pore Master 60 (Quantachrome Ltd.) over the pressure range 1–4,000 bar. On the one hand, the pore volume increases profoundly with the treatment temperature increasing (Fig. 1(a), Table 2), whereas mainly macropores ( $>0.05 \mu\text{m}$ ) are generated (Fig. 1(b)). On the other hand, the mesopores (ranging from 0.002 to  $0.05 \mu\text{m}$ ) that are evident in PI and PI-AIR-300 (Fig. 1(a)) disappear in PI-AIR-400 and PI-AIR-500, whereas the broad pore diameter distribution of PI becomes narrow for PI-AIR-300 and PI-AIR-400 and widens toward a uniform one for PI-AIR-500 (Fig. 1(b), Table 2).

The yield of derived adsorbents decreased with the temperature increasing for all gases used (Table 1). For temperatures higher than 350°C, the decrease of yield is

due to condensation of aliphatic compounds, degradation of lignocellulose structures, loss of volatiles ( $\text{CH}_4$ ,  $\text{H}_2$ ,  $\text{CO}$ ), and oxidation [25,28]. The yield is not directly related to the

Table 1  
Physical properties of raw pistachio shell (PI) and derived adsorbents

Adsorbent	Activation gas and final temperature	Yield (%)	Surface area ( $\text{m}^2/\text{g}$ )
PI	–	100	0.48
PI- $\text{N}_2$ -300	$\text{N}_2$ , 300°C	46	0.70
PI- $\text{N}_2$ -400	$\text{N}_2$ , 400°C	26	0.77
PI- $\text{N}_2$ -500	$\text{N}_2$ , 500°C	22	2.52
PI- $\text{CO}_2$ -300	$\text{CO}_2$ , 300°C	45	0.51
PI- $\text{CO}_2$ -400	$\text{CO}_2$ , 400°C	28	0.57
PI- $\text{CO}_2$ -500	$\text{CO}_2$ , 500°C	24	2.1
PI-AIR-300	Air, 300°C	35	0.99
PI-AIR-400	Air, 400°C	11	4.2
PI-AIR-500	Air, 500°C	0.5	14.5

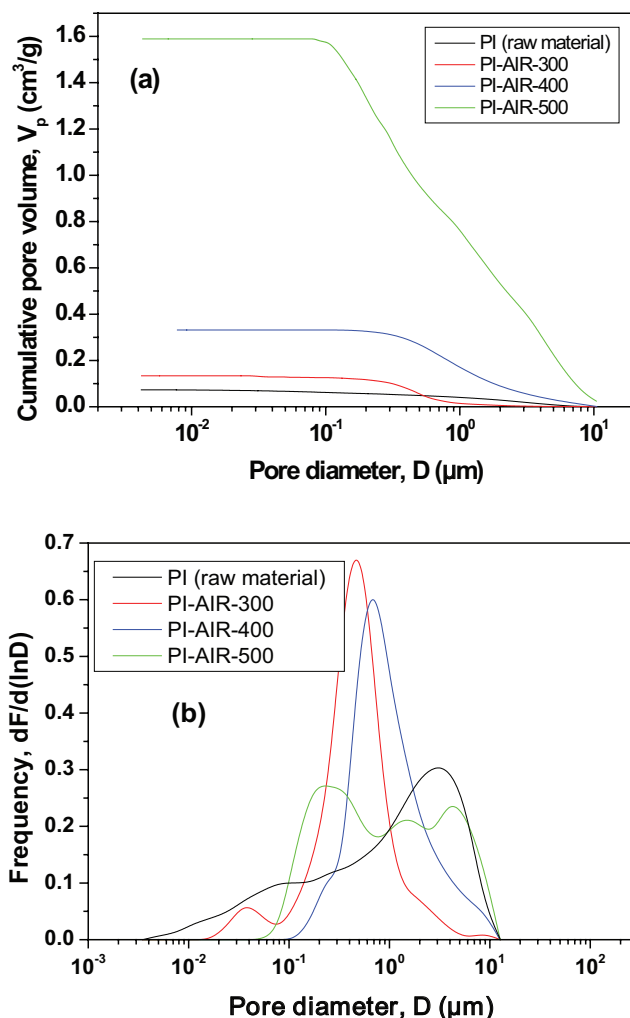


Fig. 1. (a) Cumulative pore diameter distributions of adsorbents and (b) normalized pore diameter distributions of adsorbents.

Table 2  
Properties of the pore structure of air-activated adsorbents

Adsorbent	Pore volume, $V_p$ (cm <sup>3</sup> /g)	Mean value of PSD, $\langle D \rangle$ ( $\mu\text{m}$ )	Standard deviation of PSD, $\sigma_D$ ( $\mu\text{m}$ )
PI	0.0730	0.780	5.57
PI-AIR-300	0.1338	0.424	2.40
PI-AIR-400	0.3315	0.950	2.24
PI-AIR-500	1.5889	0.890	3.77

capacity of adsorbents to adsorb heavy metals, but it is an important cost factor related to the quantity of material that can be utilized per unit mass of treated waste.

### 3.2. FTIR analysis of the surface of adsorbents

The FTIR spectra of the raw PI and air-activated adsorbents are shown in Fig. 2(a), and the FTIR spectra band assignments are presented in Table 3. Some peaks that are visible in the FTIR-spectrum of PI disappeared or appeared at low intensities in the air-produced adsorbents, indicating the removal of some functional groups as the activation temperature increased. On the other hand, the new peaks appeared for PI-AIR-400 and PI-AIR-500 in the region 600–900 cm<sup>-1</sup> are associated with aromatic and heteroaromatic compounds and were confirmed by C–H wagging vibrations. The characteristic band appeared at 875 cm<sup>-1</sup> is assigned to the aromatic C–H out-of-plane bending vibrations and was much more intensive at 500°C than at lower heating temperatures (300°C and 400°C). The sharp peak shown at 1,031 cm<sup>-1</sup> in PI, which shifts to 1,065 cm<sup>-1</sup> for all oxidized adsorbents, and the smaller peaks at around 1,014 cm<sup>-1</sup> in PI-AIR-400 and PI-AIR-500 are due to aliphatic ether, alcohol C–O or aromatic stretching, O–H deformation vibrations, or  $\beta$ -glycosidic bonds in cellulose and hemicellulose. These functional groups almost disappeared at temperatures higher than 300°C indicating the decomposition of hemicelluloses and cellulose [25,29] in agreement with results from TGA analysis (see discussion in section 3.5). The skeletal C=C vibrations in aromatic rings or aromatic C=O ring stretching (likely –COOH), which correspond to the bands at around 1,598 and 1,435 cm<sup>-1</sup> (in PI-AIR-500 shifted to the very intense band at 1,420 cm<sup>-1</sup>), were amplified in the produced adsorbents and are associated with higher alkalinity, which is expected to enhance Zn removal efficiency. The band at 1,730 cm<sup>-1</sup> for PI (shifted slightly to 1,711 cm<sup>-1</sup> for PI-AIR-300 and PI-AIR-400), which is assigned to  $\nu(\text{C}=\text{O})$  vibration in carbonyl group or the presence of carboxylic bonds (Table 3), disappeared for PI-AIR-500 due to the decomposition of carbonate compounds.

The FTIR spectra of the raw PI and produced adsorbents at 400°C under air, N<sub>2</sub>, or CO<sub>2</sub> atmosphere are shown in Fig. 2(b). The sharp peak observed at 1,031 cm<sup>-1</sup> for PI, appeared at very low intensities for PI-AIR-400 and PI-N<sub>2</sub>-400 (shifted to 1,065 and 1,080 cm<sup>-1</sup>, respectively), and disappeared for PI-CO<sub>2</sub>-400. This can be attributed to cellulose and hemicellulose decomposition at higher temperatures (see also TGA analysis in section 3.5), [25,29]. The band at 1,730 cm<sup>-1</sup> for PI (shifted to 1,711 and 1,696 cm<sup>-1</sup> for PI-AIR-400 and PI-N<sub>2</sub>-400/PI-CO<sub>2</sub>-400, respectively) is assigned to  $\nu(\text{C}=\text{O})$

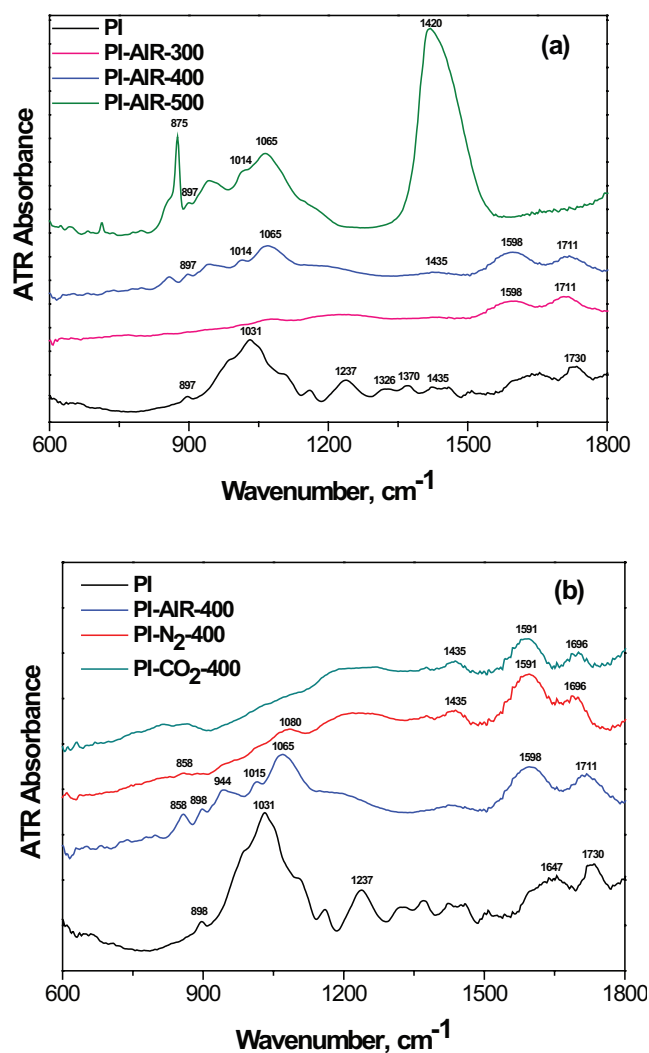


Fig. 2. FTIR spectra of raw pistachio shell (PI) and adsorbents activated by (a) air at various temperatures and (b) various gases at 400°C.

vibration in carbonyl group or the presence of carboxylic bonds (Table 3).

### 3.3. SEM analysis

Representative FE-SEM images of the morphology of the (i) raw PI, (ii) air-activated adsorbents over the temperature range 300°C–500°C (i.e., PI-AIR-300, PI-AIR-400, PI-AIR-500), and (iii) N<sub>2</sub>- and CO<sub>2</sub>-activated adsorbents at 400°C (i.e., PI-N<sub>2</sub>-400 and PI-CO<sub>2</sub>-400) are shown in Fig. 3. The presence of macropores becomes more evident as the temperature of air-treated adsorbents increases (Fig. 3), in agreement with the results of MIP (Fig. 1(a)), due mainly to the release of volatile compounds and carbon burn-off.

### 3.4. XRD analysis

More detailed structural information is provided by XRD. Diffraction patterns over a wide-angle range for the raw PI and adsorbents are shown in Fig. 4. No well-defined

Table 3  
FTIR band assignments

Band number, $\text{cm}^{-1}$	Assignment
1,730, 1,711, 1,696	C=O stretching in carbonyl groups or presence of carboxylic bonds [25,30]
1,647, 1,598, 1,591	C=C stretching in aromatic rings or aromatic C=O ring stretching [31]
1,560–1,330	Aromatic C=O stretching [30]
1,435, 1,420	C=C stretching in aromatic rings [30]
1,370, 1,326	C–O stretching in carboxylate groups (alkanes and alkyl groups) [32]
1,300–900	$\nu(\text{C–O})$ vibrations in alcohols, phenols, or ether or ester groups [30]
1,237	C=C stretching [33]
1,080, 1,065, 1,031, 1,014	C–O stretching vibrations in alcohols, aliphatic ether, O–H deformation vibrations, $\beta$ -glycosidic bond in cellulose, and hemicellulose [25,29]
900–600	C–H wagging vibrations [34]
897, 875	C–H out-of-plane bendings in benzene derivatives [32]

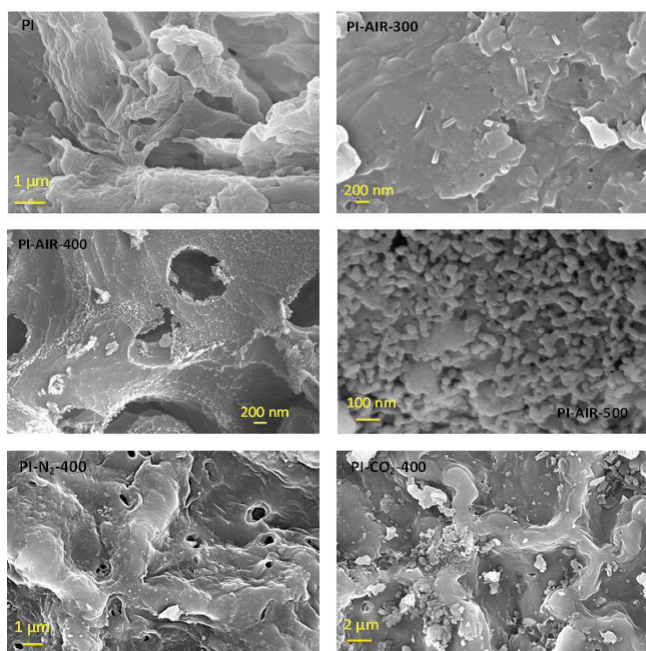


Fig. 3. Representative FE-SEM images of raw PI and produced adsorbents.

peaks are evident in the XRD spectra of PI, PI-AIR-300, PI-AIR-400, PI-N<sub>2</sub>-400, and PI-CO<sub>2</sub>-400, indicating that their structure is completely amorphous as it is also expected for organic materials. Cellulose, comprising one of the main components of the raw PI, was detected in PI, whereas the hump in the  $2\theta$  range 18°–28° was indicative of the organic matter present in PI-AIR-300, PI-AIR-400, PI-N<sub>2</sub>-400, and PI-CO<sub>2</sub>-400. Thermonatrite, resulting from the evaporation of sodium carbonate in atmospheric air, was also detected in

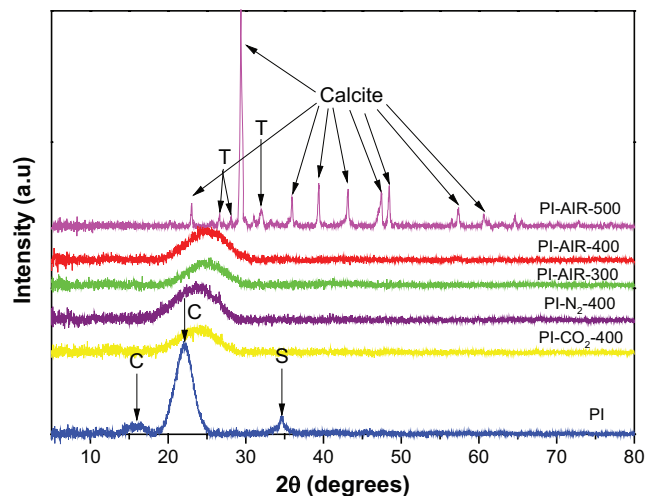


Fig. 4. XRD patterns of PI and produced adsorbents (C: cellulose-(C<sub>6</sub>H<sub>10</sub>O<sub>5</sub>)<sub>n</sub>; S: thermonatrite-Na<sub>2</sub>CO<sub>3</sub>H<sub>2</sub>O, T: tilleyite-Ca<sub>3</sub>Si<sub>2</sub>O<sub>7</sub>(CO<sub>3</sub>)<sub>2</sub>; calcite-CaCO<sub>3</sub>).

PI, but was not present in the adsorbents due to the higher activation temperature. In the case of PI-AIR-500, many new sharp peaks were observed corresponding to calcite and tilleyite mineral phases, which comprise the residual crystalline phase remaining after the treatment of PI in air at 500°C.

### 3.5. TGA/DTG analysis

The thermal stability of the raw PI was analyzed by TGA/DTG and is depicted in Fig. 5. The weight of PI was reduced by <10% up to 250°C and then was reduced steeply reaching a weight loss ~65% at temperature ~330°C (Fig. 5(a)). At higher temperatures, a slower decrease in the weight of PI was observed until the material being almost vanished (weight loss ~99.5%) at temperature ~480°C (Fig. 5(a)).

The DTG curve of PI (Fig. 5(b)) revealed three distinct peaks at 275°C, 305°C, and 481°C, corresponding to the decomposition of hemicellulose, cellulose, and lignin, respectively. Hemicellulose, cellulose (its presence also confirmed by XRD analysis), and lignin are the main components of PI, decomposing over the temperature ranges 150°C–350°C, 275°C–350°C, and 300°C–500°C, respectively [25].

### 3.6. Effect of activation gas on Zn removal efficiency

The removal of Zn<sup>2+</sup> from aqueous solutions was tested with adsorbents activated under inert (i.e., nitrogen) and oxidizing (i.e., carbon dioxide and air) atmosphere at 400°C with HR 5°C/min and HT 60 min.

The adsorption capacity of the raw PI as compared with the corresponding one of adsorbents activated at 400°C is shown in Fig. 6. For an initial Zn<sup>2+</sup> concentration equal to 100 mg/L and acidic conditions (i.e., pH = 3.7), the Zn<sup>2+</sup> removal efficiency was 22%, 21%, 18%, and 50% for PI, PI-N<sub>2</sub>-400, PI-CO<sub>2</sub>-400, and PI-AIR-400, respectively. Evidently, the Zn adsorption capacity of N<sub>2</sub>- and CO<sub>2</sub>-activated PI at 400°C did not change respectably (Fig. 6). This is consistent with the SEM images (Fig. 3) and BET data (Table 1) where no significant changes

were observed in either the pore structure or the specific surface area, when the raw material was activated under  $N_2$  and

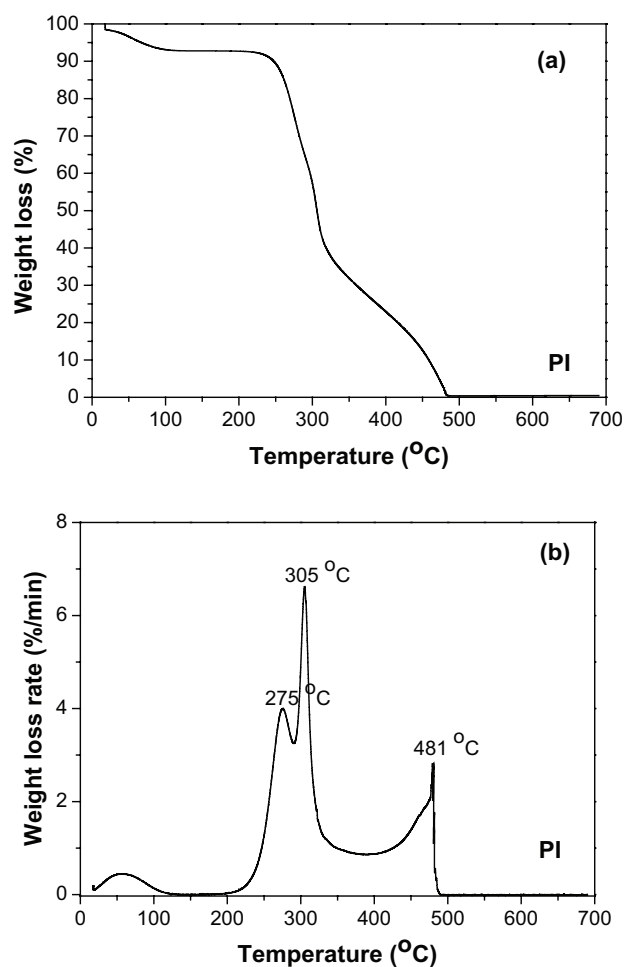


Fig. 5. Temperature programmed gravimetric analysis of raw PI: (a) Thermogravimetric curve of weight loss as a function of temperature and (b) DTG curve of weight loss rate as a function of temperature.

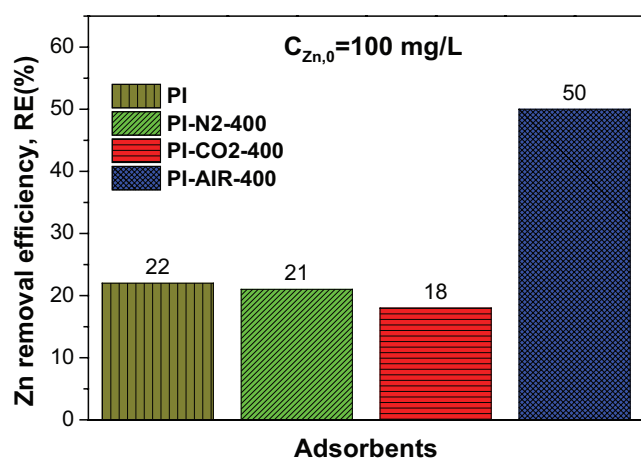


Fig. 6. Zn removal efficiency of raw PI and adsorbents activated at 400°C (heating rate = 5°C/min, holding time = 60 min).

$CO_2$  at 400°C. In addition, no functional groups favoring the Zn adsorption were detected in FTIR spectra (Fig. 2(b)).

On the other hand, the Zn removal efficiency increased from 22% to 50% for air-activated PI at 400°C. This is consistent with the higher specific surface area (Table 1) and pore volume (Table 2) of PI-AIR-400, compared with the corresponding properties of PI. Furthermore, it seems that the Zn removal efficiency is favored by the higher alkalinity caused by the presence of aromatic/heteroaromatic groups on the surface of PI-AIR-400 (Fig. 2) triggering the Zn sorption on the pore surface, and reflected in the higher final pH value of the aqueous solution, measured at the end of adsorption (Table 4).

### 3.7. Effect of activation temperature on Zn removal efficiency

The effect of activation temperature on the Zn adsorption capacity of the air-activated adsorbents is shown in Fig. 7(a). The Zn removal efficiency increased with the increasing activation temperature. In particular, the Zn removal efficiency increased from 22% (PI) to 36%, 50%, and 98% at 300°C, 400°C, and 500°C, respectively. This is in agreement with the corresponding increase of the surface area (Table 1) and pore volume (Table 2). In addition, the aromatic/heteroaromatic compounds, detected at wave numbers  $<900\text{ cm}^{-1}$  (PI-AIR-400, PI-AIR-500), and the oxygen-rich functional groups (e.g.,  $-COOH$ ,  $-C=O$ ), detected at wave number  $\sim 1,400\text{ cm}^{-1}$  (PI-AIR-500; Fig. 2(a)), favor the higher surface alkalinity associated with enhanced Zn sorption capacity of adsorbents.

It is worth mentioning that the removal efficiency of the  $N_2$ - and  $CO_2$ -activated adsorbents was independent of the activation temperature (ranging from 300°C to 500°C). The Zn removal efficiency of PI-N<sub>2</sub>-300, PI-N<sub>2</sub>-400, and PI-N<sub>2</sub>-500 varied in the range 19%–21%, whereas the corresponding one of PI-CO<sub>2</sub>-300, PI-CO<sub>2</sub>-400, and PI-CO<sub>2</sub>-500 varied in the range 17%–18% (Figs. 7(b) and (c)). Therefore, regarding the high Zn concentration ( $\sim 100\text{ mg/L}$ ) solutions, the Zn removal efficiency of  $N_2$ - and  $CO_2$ -activated adsorbents was comparable with that of raw material (PI). This is consistent with (i) the negligible increase of the specific surface area of  $N_2$ - and  $CO_2$ -activated adsorbents compared with that of PI (Table 1) over the temperature range 300°C–500°C and (ii) the FTIR

Table 4  
pH of the aqueous solution before and after the adsorption process (Zn initial concentration: 100 mg/L)

Adsorbent	pH initial	pH final	Zn removal efficiency (%)
PI	3.7	4.4	22
PI-N <sub>2</sub> -300	3.7	4.2	19
PI-N <sub>2</sub> -400	3.7	4.3	21
PI-N <sub>2</sub> -500	3.7	4.2	19
PI-CO <sub>2</sub> -300	3.7	4.2	17
PI-CO <sub>2</sub> -400	3.7	4.2	18
PI-CO <sub>2</sub> -500	3.7	4.2	17
PI-AIR-300	3.7	4.5	36
PI-AIR-400	3.7	4.8	50
PI-AIR-500	3.7	5.5	98

spectra, where no functional groups favoring the Zn adsorption were formed up to 400°C, under N<sub>2</sub> or CO<sub>2</sub> atmospheres (Fig. 2(b)).

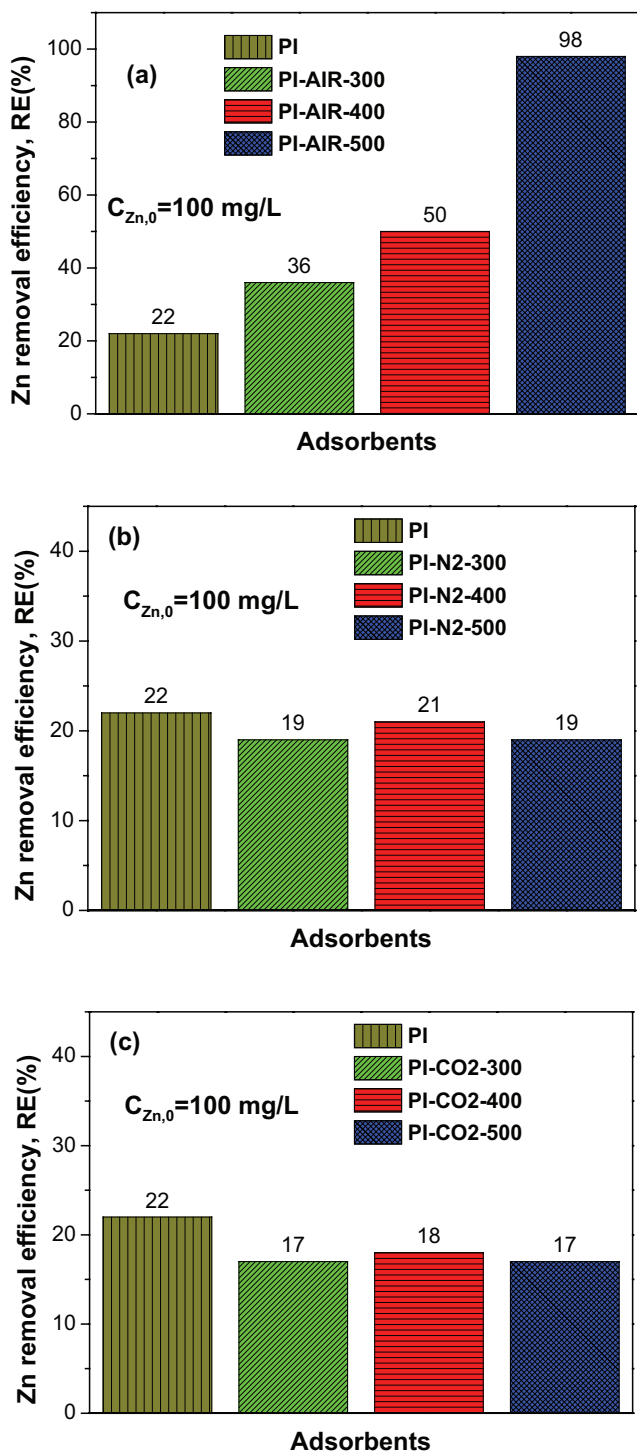


Fig. 7. Zn removal efficiency of: (a) raw PI and air-activated adsorbents; (b) raw PI and N<sub>2</sub>-activated adsorbents; and (c) raw PI and CO<sub>2</sub>-activated adsorbents (heating rate = 5°C/min, holding time = 60 min).

### 3.8. Effect of holding time and heating rate on Zn removal efficiency

PI were activated at 300°C and 400°C under air atmosphere for two HRs (5°C/min and 10°C/min) and two HTs (30 and 60 min) to examine potential effects of heating parameters on the Zn removal efficiency.

The Zn removal efficiency increased with the HT increasing for air-activated adsorbents at 300°C and 400°C (Fig. 8(a)), but no sensible change was observed with respect to the HR (Fig. 8(b)).

### 3.9. Zn sorption isotherms

Due to the very low yield (~0.5%) of the most efficient adsorbent (i.e., PI-AIR-500) that minimizes its practical use, no additional studies were done for PI-AIR-500, and all subsequent tests were limited on the next most efficient adsorbent: PI-AIR-400. The sorption isotherms of Zn on the raw PI and PI-AIR-400 (HR = 5°C/min, HT = 60 min) are shown in Fig. 9. The removal efficiency of both adsorbents increased with the decreasing initial metal concentration, with the adsorption capacity of the air-activated adsorbent (i.e., PI-AIR-400)

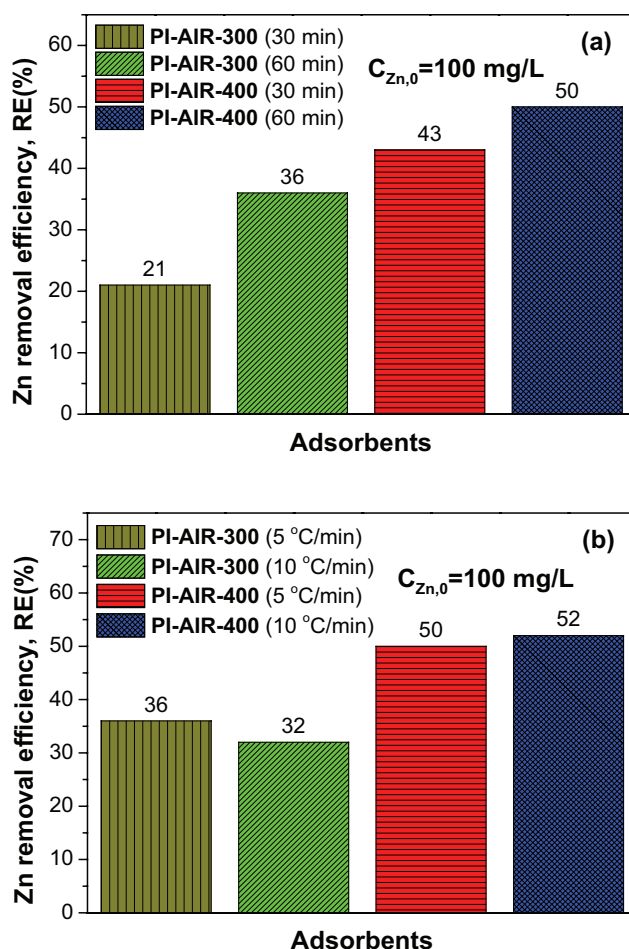


Fig. 8. Zn removal efficiency as a function of (a) holding time (heating rate: 5°C/min) and (b) heating rate (holding time: 60 min).

being always higher than that of PI. The Zn removal efficiency of PI-AIR-400 was respectable (>85%) even over high initial Zn concentrations (i.e., 80 mg/L) compared with that of PI (~33%). At the lowest initial Zn concentration (i.e., 5 mg/L), the Zn removal efficiency of PI and PI-AIR-400 was 76% and 96%, respectively. It is worth mentioning that for initial Zn concentrations in the range 5–20 mg/L, the PI-AIR-400 was able to remove more than 93% of the initial Zn from aqueous solutions (Fig. 9).

The sorption isotherms of Zn for the PI and PI-AIR-400 were fitted with Langmuir and Freundlich models. The Langmuir model assumes that the adsorbent surface is homogeneous, the species sorption on its surface is monolayer, no interaction between adsorbed molecules occurs, and it is described by the following equation [35,36]:

$$q_e = \frac{QbC_e}{1 + bC_e} \quad (3)$$

where  $q_e$  (mg/g) is the amount of metal adsorbed per unit mass of adsorbent;  $C_e$  (mg/L) is the equilibrium concentration of metal ion in solution;  $Q$  (mg/g) is the maximum adsorption capacity of the adsorbent; and  $b$  (L/mg) is the Langmuir adsorption constant related to binding energies. In the case of Zn adsorption onto both PI and PI-AIR-400, the fitting of the experimental data with this model was satisfactory (Fig. 10(a), Table 5). Moreover, the monolayer adsorption capacity of Zn, as quantified by the parameter  $Q$ , was found equal to 2.564 and 5.236 mg/g for PI and PI-AIR-400, respectively (Table 5), revealing the higher monolayer adsorption capacity of PI-AIR-400.

On the other hand, the Freundlich model describes the heterogeneous multi-layer species sorption upon adsorbent [36,37]; it is decomposed into a number of Langmuir component isotherms; and it is described by the relation:

$$q_e = KC_e^{1/n} \quad (4)$$

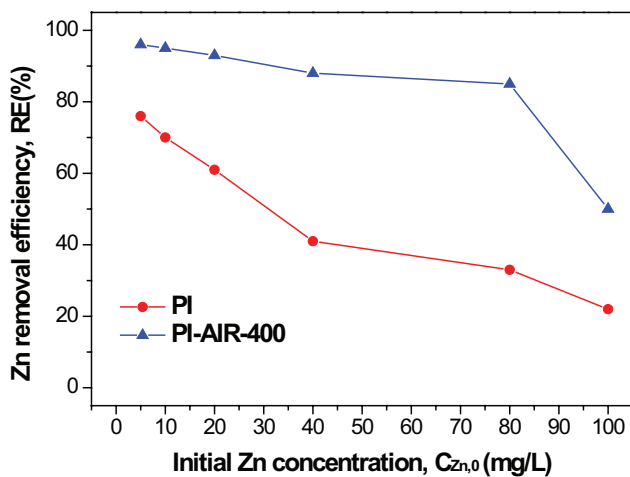


Fig. 9. Zn removal efficiency as a function of initial Zn concentration for raw PI and air-activated adsorbents at 400°C (PI-AIR-400).

where  $K$  ((mg/g)(L/mg)<sup>1/n</sup>) is a constant related to the maximum adsorption capacity of the adsorbent, and  $1/n$  is a constant related to the strength of adsorption. Based on  $1/n$  Freundlich exponent (Table 5), the adsorption of Zn on PI and PI-AIR-400 is regarded as a favorable process ( $1/n < 1$ ), indicating that the adsorption bond is strong. In the case of air-activated adsorbents at 400°C (PI-AIR-400), the

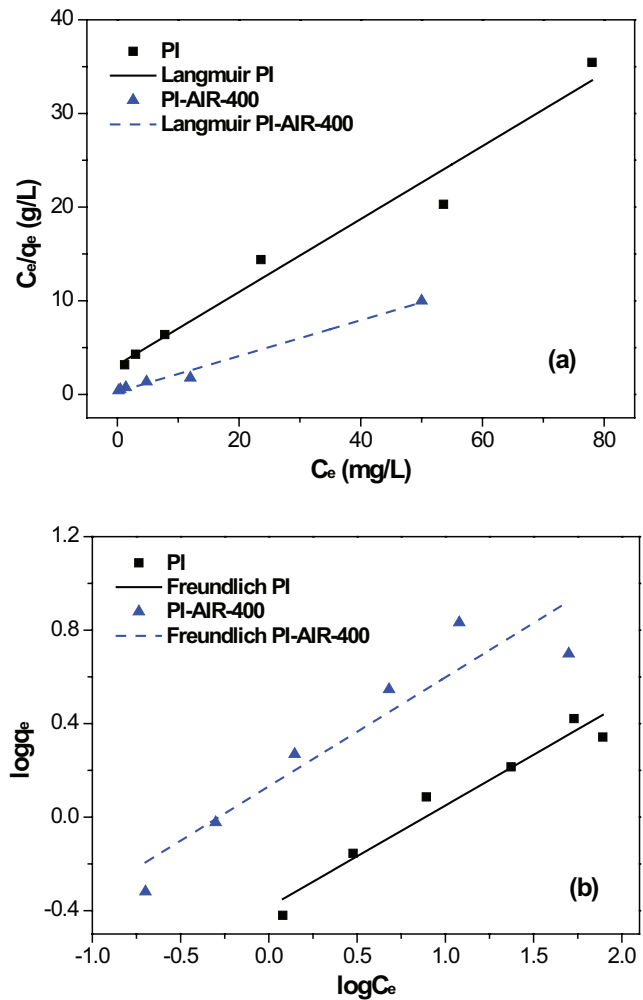


Fig. 10. Fitting of Zn sorption isotherms to (a) Langmuir and (b) Freundlich models for raw PI and air-activated adsorbents at 400°C (PI-AIR-400).

Table 5  
Estimated parameter values and correlation coefficients of Langmuir and Freundlich sorption models for the raw PI and air-activated adsorbent at 400°C (PI-AIR-400)

Model	Langmuir model			Freundlich model		
	Linearized equation	$\frac{C_e}{q_e} = \frac{1}{Qb} + \frac{C_e}{Q}$	$\log q_e = \log K + \frac{1}{n} \log C_e$	$K$	$1/n$	$R^2$
Adsorbent	$Q$	$b$	$R^2$	$K$	$1/n$	$R^2$
PI	2.564	0.124	0.964	0.412	0.435	0.940
PI-AIR-400	5.236	0.692	0.986	1.355	0.466	0.848

Freundlich model fits also satisfactorily to the experimental data (Fig. 10(b), Table 5).

### 3.10. Correlation of adsorbent properties with sorption mechanisms

Physical or surface sorption describes the removal of heavy metals by diffusional movement of metal ions into sorbent pores without formation of chemical bonds. The high surface areas and pore volumes of adsorbents favor the diffusive surface adsorption process [38]. The pore volume (Table 2) and specific surface area (Table 1) increase sensibly for PI-AIR-400 and PI-AIR-500 and may explain the higher Zn removal efficiency through physical sorption.

The abundance of oxygen containing groups (C=O, C–O, OH) in air-activated adsorbents (Fig. 2, Table 3) may provide negatively charged surface sites (COO<sup>-</sup> and OH<sup>-</sup>) that favor the electrostatic attraction of Zn<sup>2+</sup> [39].

Metals and rare earth elements with intermediate ionization potentials between 2.5 and 9.5 (e.g., Cu, Zn, Ni, Pb) are more likely to precipitate on adsorbent surfaces than other elements. Normally, under acidic conditions (pH < 5), no Zn precipitation on adsorbent surface is expected to occur [39]. However, except of the higher alkalinity, precipitation of heavy metals may arise from the reaction of metallic ions with several mineral phases entrained in biomass. LCAs produced at high temperatures have high mineral matter content with significant levels of Ca, Mg, Fe, Cu, and Si elements. These mineral phases may include quartz (SiO<sub>2</sub>), amorphous silica, calcite (CaCO<sub>3</sub>), hydroxyapatite, and calcium anhydrite (CaSO<sub>4</sub>), either in free form or intercalated within the carbon matrix of the LCA [38]. The less soluble forms of these mineral phases are generated at higher temperatures (350°C–600°C), and are more likely to be slowly released during sorption reactions with heavy metals to form precipitates on LCA surface [38]. Therefore, the high Zn removal efficiency observed for PI-AIR-500 (Fig. 7(a)) might be attributed not only to higher specific surface area and pore volume but also to Zn precipitation on the pore surface stimulated by the high percentage of calcite (Fig. 4).

Complexation (outer and inner sphere) involves the formation of multi-atom structures (i.e., complexes) with specific metal–ligand interactions. In particular, oxygen functional groups (carboxyl, phenolic, and lactonic) in adsorbents produced in relatively low temperatures have been demonstrated to effectively bind with heavy metals [40]. Hence, the oxygen-rich functional groups (e.g., –COOH, –C=O), detected for PI-AIR-400 and PI-AIR-500 (Fig. 2, Table 3), may favor the increase of Zn sorption through complexation.

## 4. Conclusions

PI were used for the preparation of various types of adsorbents with thermal treatment over the temperature range 300°C–500°C, under inert (N<sub>2</sub>) and oxidizing (air or CO<sub>2</sub>) atmosphere. The adsorbents were evaluated with respect to their capacity to remove Zn dissolved in acidic aqueous solutions (pH < 4), where the sorption capacity of the raw material is very low. The most important conclusions are outlined below:

- SEM analysis revealed that no respectable changes on the pore structure took place when the raw material was activated under N<sub>2</sub> and CO<sub>2</sub> at 400°C. In contrast, in air-activated adsorbents, Hg porosimetry and SEM analysis measurements revealed that mainly macropores are generated and the pore volume increases sharply with the treatment temperature (300°C–500°C).
- The BET surface area increased weakly or strongly with the temperature for the N<sub>2</sub>- and CO<sub>2</sub>-activated or air-activated carbon materials, respectively.
- In the air-activated adsorbents at the highest temperatures of 400°C and 500°C, ATR-FTIR spectroscopy revealed the presence of aromatic/heteroaromatic compounds and oxygen functional groups such as aromatic C=O ring stretching (likely –COOH), both associated with higher alkalinity.
- The XRD patterns showed an amorphous structure of raw material and all activated adsorbents up to 400°C. However, a crystalline phase of calcite was identified for the air-produced adsorbent at 500°C.
- A comparative analysis of the Zn sorption capacity of adsorbents revealed that the air-activated adsorbents prepared in the temperature range 400°C–500°C were the most efficient ones. The sorption capacity of N<sub>2</sub>- and CO<sub>2</sub>-activated adsorbents was comparable with that of raw material.
- The Zn sorption capacity of air-activated adsorbents was affected positively by the activation temperature and HT and weakly by the HR.
- The characteristics of the investigated adsorbents were found fully compatible with the observed Zn sorption capacity and potential sorption mechanisms. Specifically, the enhancement of the sorption capacity of air-treated adsorbents might be due to: (i) the higher pore surface area and volume associated with physical sorption; (ii) the presence of mineral phases triggering the precipitation; and (iii) the presence of oxygen-rich functional groups associated with complexation and/or electrostatic attraction.
- The Zn sorption onto pistachio raw shells and air-activated adsorbents was fitted satisfactorily with Langmuir and Freundlich isotherms.
- The optimal conditions for the preparation of efficient LCA were the following: heating of PI in air at 400°C with a rate of 5°C/min and HT 60 min.

The cost of Zn removal from aqueous solutions, even under adverse acidic conditions (pH < 4), is expected to be low, given that the pistachio-produced LCA are activated in air with heating at a relatively low temperature (e.g., 400°C).

## Acknowledgments

This work was performed in the framework of PROENYL project within the KRIPIS action, funded by Greece, and the European Regional Development Fund of the European Union under the O.P. Competitiveness and Entrepreneurship.

## References

- [1] Ö. Demirbaş, A. Karadağ, M. Alkan, M. Doğan, Removal of copper ions from aqueous solutions by hazelnut shell, *J. Hazard. Mater.*, 153 (2008) 677–684.

- [2] A. Bhatnagar, M. Sillanpää, Utilization of agro-industrial and municipal waste materials as potential adsorbents for water treatment—a review, *Chem. Eng. J.*, 157 (2010) 277–296.
- [3] P.J.M. Carrott, M.M.L. Ribeiro Carrott, P.A.M. Mourão, R.P. Lima, Preparation of activated carbons from cork by physical activation in carbon dioxide, *Adsorpt. Sci. Technol.*, 21 (2003) 669–681.
- [4] N.H. Phan, S. Rio, C. Faur, L. Le Coq, P. Le Cloirec, T.H. Nguyen, Production of fibrous activated carbons from natural cellulose (jute, coconut) fibers for water treatment applications, *Carbon*, 44 (2006) 2569–2577.
- [5] M.A. Lillo-Ródenas, J.P. Marco-Lozar, D. Cazorla-Amorós, A. Linares-Solano, Activated carbons prepared by pyrolysis of mixtures of carbon precursor/alkaline hydroxide, *J. Anal. Appl. Pyrol.*, 80 (2007) 166–174.
- [6] N. Asasian, T. Kaghazchi, M. Soleimani, Elimination of mercury by adsorption onto activated carbon prepared from the biomass material, *J. Ind. Eng. Chem.*, 18 (2012) 283–289.
- [7] S.K. Theydan, M.J. Ahmed, Adsorption of methylene blue onto biomass-based activated carbon by FeCl<sub>3</sub> activation: equilibrium, kinetics, and thermodynamic studies, *J. Anal. Appl. Pyrolysis*, 97 (2012) 116–122.
- [8] R. Baccar, M. Sarrà, J. Bouzid, M. Feki, P. Blázquez, Removal of pharmaceutical compounds by activated carbon prepared from agricultural by-product, *Chem. Eng. J.*, 211–212 (2012) 310–317.
- [9] I. Ali, V.K. Gupta, Advances in water treatment by adsorption technology, *Nat. Protoc.*, 1 (2007) 2661–2667.
- [10] V.K. Gupta, P.J.M. Carrott, M.M.L. Ribeiro Carrott, Suhas, Low-cost adsorbents: growing approach to wastewater treatment—a review, *Crit. Rev. Env. Sci. Technol.*, 39 (2009) 783–842.
- [11] E. Agrafioti, D. Kalderis, E. Diamadopoulos, Arsenic and chromium removal from water using biochars derived from rice husk, organic solid wastes and sewage sludge, *J. Environ. Manage.*, 133 (2014) 309–314.
- [12] E.W. Shin, K.G. Karthikeyan, M.A. Tshabalala, Adsorption mechanism of cadmium on juniper bark and wood, *Bioresour. Technol.*, 98 (2007) 588–594.
- [13] F. Ferrero, Dye removal by low cost adsorbents: hazelnut shells in comparison with wood sawdust, *J. Hazard. Mater.*, 142 (2007) 144–152.
- [14] M. Dakiky, M. Khamis, A. Manassra, M. Mer'eb, Selective adsorption of chromium(VI) in industrial wastewater using low-cost abundantly available adsorbents, *Adv. Environ. Res.*, 6 (2002) 533–540.
- [15] E.-K. Guechi, O. Hamdaoui, Evaluation of potato peel as a novel adsorbent for the removal of Cu(II) from aqueous solutions: equilibrium, kinetic, and thermodynamic studies, *Desal. Wat. Treat.*, 57 (2016) 10677–10688.
- [16] E.-K. Guechi, O. Hamdaoui, Biosorption of methylene blue from aqueous solution by potato (*Solanum tuberosum*) peel: equilibrium modelling, kinetic, and thermodynamic studies, *Desal. Wat. Treat.*, 57 (2016) 10270–10285.
- [17] D. Suteu, M. Badeanu, T. Malutan, A.-I. Chirculescu, Valorization of food wastes (orange seeds) as adsorbent for dye retention from aqueous medium, *Desal. Wat. Treat.*, 57 (2016) 29070–29081.
- [18] M. Kazempour, M. Ansari, S. Tajrobehkar, M. Majdzadeh, H.R. Kermani, Removal of lead, cadmium, zinc, and copper from industrial wastewater by carbon developed from walnut, hazelnut, almond, pistachio shell, and apricot stone, *J. Hazard. Mater.*, 150 (2008) 322–327.
- [19] T. Yang, A.C. Lua, Characteristics of activated carbons prepared from pistachio-nut shells by physical activation, *J. Colloid Interface Sci.*, 267 (2003) 408–417.
- [20] A.C. Lua, T. Yang, J. Guo, Effects of pyrolysis conditions on the properties of activated carbons prepared from pistachio-nut shells, *J. Anal. Appl. Pyrolysis*, 72 (2004) 279–287.
- [21] A.C. Lua, T. Yang, Characteristics of activated carbon prepared from pistachio-nut shell by zinc chloride activation under nitrogen and vacuum conditions, *J. Colloid Interface Sci.*, 290 (2005) 505–513.
- [22] H. Dolas, O. Sahin, C. Saka, H. Demir, A new method on producing high surface area activated carbon: the effect of salt on the surface area and the pore size distribution of activated carbon prepared from pistachio shell, *Chem. Eng. J.*, 166 (2011) 191–197.
- [23] A.H. Faramarzi, T. Kaghazchi, H.A. Ebrahim, A.A. Ebrahimi, Experimental investigation and mathematical modeling of physical activated carbon preparation from pistachio shell, *J. Anal. Appl. Pyrolysis*, 114 (2015) 143–154.
- [24] N.G. Turan, B. Mesci, Use of pistachio shells as an adsorbent for the removal of zinc(II) ion, *Clean*, 39 (2011) 475–481.
- [25] K. Komnitsas, D. Zaharaki, I. Pyliotis, D. Vamvuka, G. Bartzas, Assessment of pistachio shell biochar quality and its potential for adsorption of heavy metals, *Waste Biomass Valorization*, 6 (2015) 805–816.
- [26] G. Moussavi, R. Khosravi, Preparation and characterization of a biochar from pistachio hull biomass and its catalytic potential for ozonation of water recalcitrant contaminants, *Bioresour. Technol.*, 119 (2012) 66–71.
- [27] İ. Demiral, N.G. Atilgan, S. Şensöz, Production of biofuel from soft shell of pistachio (*Pistacia vera* L.), *Chem. Eng. Commun.*, 196 (2008) 104–115.
- [28] M.J. Antal, M. Grønli, The art, science, and technology of charcoal production, *Ind. Eng. Chem. Res.*, 42 (2003) 1619–1640.
- [29] D. Angin, T.E. Köse, U. Selengil, Production and characterization of activated carbon prepared from safflower seed cake biochar and its ability to absorb reactive dyestuff, *Appl. Surf. Sci.*, 280 (2013) 705–710.
- [30] A.C. Lua, T. Yang, Effects of vacuum pyrolysis conditions on the characteristics of activated carbons derived from pistachio-nut shells, *J. Colloid Interface Sci.*, 276 (2004) 364–372.
- [31] B. Chen, Z. Chen, S. Lv, A novel magnetic biochar efficiently sorbs organic pollutants and phosphate, *Bioresour. Technol.*, 102 (2011) 716–723.
- [32] B. Esteves, A. Velez Marques, I. Domingos, H. Pereira, Chemical changes of heat treated pine and eucalypt wood monitored by FTIR, *Maderas-Cienc. Technol.*, 15 (2013) 245–258.
- [33] X. Cao, W. Harris, Properties of dairy-manure-derived biochar pertinent to its potential use in remediation, *Bioresour. Technol.*, 101 (2010) 5222–5228.
- [34] B. Glaser, L. Haumaier, G. Guggenberger, W. Zech, The 'Terra Preta' phenomenon: a model for sustainable agriculture in the humid tropics, *Naturwissenschaften*, 88 (2001) 37–41.
- [35] J. Febrianto, A.N. Kosasih, J. Sunarso, Y. Ju, N. Indraswati, S. Ismadij, Equilibrium and kinetic studies in adsorption of heavy metals using biosorbent: a summary of recent studies, *J. Hazard. Mater.*, 162 (2009) 616–645.
- [36] M. Tuzen, A. Sari, D. Mendil, M. Soylak, Biosorptive removal of mercury(II) from aqueous solution using lichen (*Xanthoparmelia conspersa*) biomass: kinetic and equilibrium studies, *J. Hazard. Mater.*, 169 (2009) 263–270.
- [37] J.U.K. Oubagaranadin, N. Sathyamurthy, Z.V.P. Murthy, Evaluation of Fuller's earth for the adsorption of mercury from aqueous solutions: a comparative study with activated carbon, *J. Hazard. Mater.*, 142 (2007) 165–174.
- [38] M.I. Inyang, B. Gao, Y. Yao, Y. Xue, A. Zimmerman, A. Mosa, P. Pullammanappallil, Y.S. Ok, X. Cao, A review of biochar as a low-cost adsorbent for aqueous heavy metal removal, *Crit. Rev. Env. Sci. Technol.*, 46 (2016) 406–433.
- [39] J. Kumar, C. Balomajumder, P. Mondal, Application of agro-based biomasses for zinc removal from wastewater – a review, *Clean*, 39 (2011) 641–652.
- [40] D. Mohan, C.U. Pittman Jr., M. Bricka, F. Smith, B. Yancey, J. Mohammad, P.H. Steele, M.F. Alexandre-Franco, V. Gomez-Serrano, H. Gong, Sorption of arsenic, cadmium, and lead by chars produced from fast pyrolysis of wood and bark during bio-oil production, *J. Colloid Interface Sci.*, 310 (2007) 57–73.